DALTON

New vanadium-(IV) and -(V) analogues of Amavadin ‡

Paul D. Smith, Robert E. Berry, Spencer M. Harben, Roy L. Beddoes, Madeleine Helliwell, David Collison and C. David Garner *,†

Department of Chemistry, The University of Manchester, Oxford Road, Manchester, UK M13 9PL

The new pro-ligand *meso*-2,2′-(hydroxyimino)dibutyric acid (*R*,*S*-H_3hidba) has been synthesised from hydroxylammonium chloride and 2-bromobutyric acid. Reaction of H_3hidba with $[VO(acac)_2]$ (acac = acetylacetonate) yielded the complex $[V(R,S\text{-hidba})_2]^{2-}$ **1**, which was crystallised in the presence of Ca^{2+} ions from H_2O as blue tabular crystals. X-Ray crystallography confirmed the same distinctive eight-co-ordinate structure of the complex anion as identified for Amavadin, the form in which vanadium(IV) is bound in *Amanita muscaria* mushrooms. The crystal structure of **1** contains a network of linked Ca and V centres where the asymmetric unit consists of a Ca_2V_2 box-like configuration. The Ca and V metal ions are bridged to one another *via* a series of unidentate and bidentate carboxylate groups from H_3hidba, extending throughout the lattice framework. The novel interaction between Ca^{2+} ions and Amavadin-style complexes has been further illustrated in the crystal structure of $[Ca(H_2O)_5][V(hida)_2]\cdot H_2O$ (H_3hida = *N*-hydroxyiminodiacetic acid) **2**. The unit cell packing arrangement observed for **2** differs from **1**, comprising helical chains formed by alternate Ca and V units linked only by unidentate carboxylate groups. Cyclic voltammetric studies of **1** exhibited a reversible V^{V}–V^{IV} redox couple in H_2O ($E_{\frac{1}{2}} = +0.43$ V, *vs.* saturated calomel electrode), this oxidation potential is considerably lower in organic solvents (*e.g.* Me_2SO, $E_{\frac{1}{2}} = -0.07$ V). The chemical oxidation of **1** in aqueous medium by ammonium ceric nitrate produced a dark red solution which was transferred into CH_2Cl_2 using $[PPh_4]Br$. From this solution $[PPh_4][V(R,S\text{-hidba})_2]$ **3** was isolated and studied using ^1H, ^{13}C and ^{51}V NMR spectroscopy. The cyclic voltammogram of **3** also displays a reversible V^{V}–V^{IV} redox couple in CH_2Cl_2 ($E_{\frac{1}{2}} = -0.09$ V).

Mushrooms of the genus *Amanita* accumulate vanadium to concentrations of up to 400 mg kg^{-1} (dry weight)[1] in the form of the discrete moiety Amavadin.[2] This contains a 1 : 2 complex of vanadium(IV) with *S*,*S*-H_3hidpa [H_3hidpa = 2,2′-(hydroxyimino)dipropionic acid].[3,4] Initially an X-ray crystallographic study of $[NH_4][NMe_4][V(hida)_2]$ (H_3hida = *N*-hydroxyiminodiacetic acid) established the unusual eight-co-ordination of the complex anion, with each $hida^{3-}$ ligand bonding *via* the η^2-NO group and two unidentate carboxylate groups.[5] Both Amavadin and its H_3hida analogue undergo a reversible one-electron V^{V}–V^{IV} redox couple,[6,7] for each case a reduction of ≈500 mV is observed in this redox couple between values recorded in H_2O and Me_2SO. Further studies[8,9] into the chemical nature of Amavadin have established the same unique eight-co-ordinate geometry identified for $[NH_4][NMe_4][V(hida)_2]$.[5] Both the vanadium-(IV) and -(V) forms of Amavadin have been crystallographically characterised as $H_2[V(S,S\text{-hidpa})_2]\cdot 4H_2O$[8] and $[PPh_4][V(S,S\text{-hidpa})_2]$,[9] respectively. Complementary work[9,10] has included the analogous $[PPh_4][V(hida)_2]$ compound which further established this distinctive eight-co-ordination where vanadium(V) is bound to two mutually *trans* η^2-NO groups and four unidentate carboxylates. This co-ordination environment leads to chirality at the vanadium (Scheme 1) and the isolated natural product Amavadin consists of an approximately equimolar mixture of the Δ- and Λ-helical forms of $[V(S,S\text{-hidpa})_2]^{2-}$.[8,9] These complexes are assigned idealised C_2 point symmetry, where the two-fold axis bisects the normals to the {VNO} plane from each ligand projected through the metal atom. The biological role of Amavadin has not yet been established beyond any doubt, however, there is considerable circumstantial evidence that suggests it could be involved as an electron-transfer mediator for the electrocatalytic oxidation of thiols[7,12] and phenols.[7] The unique geometry and chemical behaviour of Amavadin has generated curiosity as to whether it is possible to extend this chemistry. Recent studies have produced a range of new Amavadin-style complexes with other metals, such as molybdenum,[13,14] niobium,[15] tantalum,[15] titanium[16] and zirconium.[16] New work reported in this paper has explored possible variations on the H_3hidpa pro-ligand leading to the synthesis of *R*,*S*-H_3hidba [*meso*-2,2′-(hydroxyimino)dibutyric acid], where the methyl substituents on H_3hidpa have been exchanged for ethyl groups. This pro-ligand has been complexed to vanadium-(IV) and -(V), and this paper details the structural and redox properties of this new variation in this unusual eight-co-ordinate family of complexes. The use of Ca^{2+} counter ions to form extended lattices with the complex anions will be described.

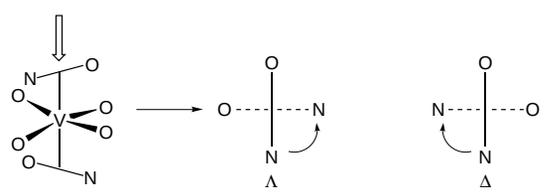

Scheme 1 Chirality at the vanadium centre viewed down the η^2-NO bonds which gives rise to the Λ- and Δ-helical forms

Experimental

Reagents and apparatus

All reagents and solvents were obtained from normal commercial sources and were used without further purification unless otherwise stated. Tetrahydrofuran (thf) and Et_2O were distilled from sodium and CH_2Cl_2 was distilled from CaH_2, and all solvents were stored under dinitrogen prior to use.

The pro-ligand *N*-hydroxyiminodiacetic acid (H_3hida) was

† E-Mail: dave.garner@manchester.ac.uk

‡ *Non-SI unit employed:* G = 10^{-4} T.

synthesised using a modified procedure[15] based on the method described by Felcman *et al.*[17] Purification was carried out using the procedure outlined by Koch and co-workers.[18]

Chemical analyses were performed by The University of Manchester, Microanalytical Laboratory. Infrared spectra were recorded on a Perkin-Elmer 1710 FT spectrometer. Electronic absorption spectra were recorded on a Varian Cary 1E UV/VIS spectrophotometer. Proton ^{13}C and ^{51}V NMR spectra were measured using a Bruker AC 300 spectrometer. Mass spectra were recorded using a KRATOS concept 1S spectrometer (matrix *m*-nitrobenzyl alcohol). The negative-ion FAB mass spectral data quoted correspond to the largest peak observed assigned to the molecular anion. Electrochemical measurements were made with a PAR model 175 waveform generator, a model 173 potentiostat and a PAR electrochemistry cell with a three-electrode configuration consisting of a platinum bead working electrode, a saturated calomel reference electrode (SCE) and a platinum wire secondary electrode. Data were recorded on an Advance Bryans series 6000 xy/t recorder. The cyclic voltammograms were recorded for solutions of compound (*ca.* 1 mmol dm^{-3}) with $[NBu^n_4][BF_4]$ (*ca.* 0.2 mol dm^{-3}) as supporting electrolyte in non-aqueous media; this salt was prepared from $Na[BF_4]$ and $[NBu^n_4][HSO_3]$ and recrystallised from toluene.[19] Potassium chloride (*ca.* 0.2 mol dm^{-3}) was used as supporting electrolyte for cyclic voltammograms recorded in H_2O. All solutions were deoxygenated by bubbling dinitrogen through them for several minutes prior to use and all voltammograms were recorded with solutions under a dinitrogen atmosphere at 293 K. All electrochemical potentials were measured relative to SCE and were corrected for liquid-junction potentials in non-aqueous media *via* the use of the ferrocenium–ferrocene couple as an internal redox standard.[20]

Syntheses

***meso*-2,2′-(Hydroxyimino)dibutyric acid, *R*,*S*-H_3hidba·0.5 H_2O.** Hydroxylammonium chloride (3.5 g, 0.05 mol), previously neutralised with 5 mol dm^{-3} NaOH (10 cm^3), was added dropwise to *R*,*S*-2-bromobutyric acid (16.7 g, 10.6 cm^3, 0.100 mol), also previously neutralised with 5 mol dm^{-3} NaOH (20 cm^3). One equivalent of 5 mol dm^{-3} NaOH (20 cm^3) was added, keeping the temperature of the reaction mixture below 278 K at all times and it was then left to stand (*ca.* 72 h) at 275 K. After this period the clear solution was acidified to *ca.* pH 2 with 5 mol dm^{-3} HCl and then evaporated to dryness under vacuum. The resultant white residue was extracted into thf (50 cm^3), subjected to ultrasound (*ca.* 30 min) and filtered to remove the salts (NaCl, NaBr) that had been precipitated. The thf solution was evaporated to dryness under vacuum where the resultant white residue was dissolved in H_2O (100 cm^3) and treated with an acidic ion-exchange resin (Amberlite IR-120). This solution was then reduced in volume under vacuum (*ca.* 15 cm^3) and left to stand (*ca.* 48 h) at 275 K. A white precipitate formed which was collected by filtration and washed with ice-cold H_2O (10 cm^3). This white product was dissolved in MeOH (10 cm^3) and H_2O (5 cm^3) added; from the resulting clear solution white needle-like crystals were obtained by slow evaporation (*ca.* 48 h) at 293 K, which were collected and dried under vacuum. Yield 3.47 g, 34% (Found: C, 44.75; H, 7.72; N, 6.39. Calc. for $C_{16}H_{32}N_2O_{11}$: C, 44.85; H, 7.53; N, 6.54%). IR (KBr, cm^{-1}): 1709 [ν(C=O)], 1462 [ν(C–O)] and 1216 cm^{-1} [ν(N–O)]. NMR (CD_3OD, 293 K): ^1H, δ 3.68 (t, 2 H, CH, $^3J_{HH}$ = 7), 1.94 (dq, 4 H, CH_2, $^3J_{HH}$ = 7, $^3J_{HH}$ = 7) and 1.07 (t, 6 H, CH_3, $^3J_{HH}$ = 7 Hz); ^{13}C, δ 175.29 (CO_2H), 69.73 (CH), 23.75 (CH_2) and 10.61 (CH_3). Mass spectrum (EI): *m*/*z* 206, H[H_3hidba)], H{NOH-[$CH(CH_2CH_3)CO_2H]_2$}.

[$Ca(H_2O)_2$][Δ,Λ-V(*R*,*S*-hidba)$_2$]·0.5 H_2O·0.5 Pr^iOH 1. The compound $[VO(acac)_2]$ (acac = acetylacetonate) (265 mg, 1.00 mmol) was added to a solution of *R*,*S*-H_3hidba (431 mg, 2.10 mmol) in MeOH (5 cm^3) and H_2O (10 cm^3). The reaction mixture was stirred (*ca.* 1 h) at 293 K, whereupon a blue-purple solution formed. Calcium chloride (111 mg, 1.00 mmol) was added and stirring continued (*ca.* 1 h). Blue tabular crystals were obtained from this MeOH–H_2O solution *via* the slow vapour-diffusion technique using Pr^iOH at 293 K. Yield 385 mg, 68% (Found: 38.0; H, 5.8; Ca, 6.9; N, 4.9; V, 8.8. Calc. for **1**, $C_{35}H_{66}Ca_2N_4O_{26}V_2$: C, 37.4; H, 5.9; Ca, 7.1; N, 5.0; V, 9.1%). IR (KBr, cm^{-1}): 1613 [ν(C=O)], 1386 [ν(C–O)] and 1140 cm^{-1} [ν(N–O)]. UV/VIS (H_2O): ν/cm^{-1} (ε/dm^3 mol^{-1} cm^{-1}) 17 800 (25.3), 13 900 (15.2), 12 900 (14.8). Mass spectrum (negative-ion FAB): *m*/*z* 456, H[V(hidba)$_2$]$^-$.

[$Ca(H_2O)_5$][Δ,Λ-V(hida)$_2$]·H_2O 2. The compound was prepared as for **1** with $[VO(acac)_2]$ (265 mg, 1.00 mmol), H_3hida (315 mg, 2.11 mmol) and $CaCl_2$ (111 mg, 1.00 mmol) in H_2O (10 cm^3). Blue prismatic crystals were obtained from H_2O–Pr^iOH *via* the slow liquid-diffusion technique at 293 K. Yield 447 mg, 91% (Found: C, 20.21; H, 3.9; Ca, 8.46; N, 5.71; V, 10.14. Calc. for $C_8H_{20}CaN_2O_{16}V$: C, 20.3; H, 3.83; Ca, 8.47; N, 5.92; V, 10.76%).

[PPh_4][Δ,Λ-V(*R*,*S*-hidba)$_2$] 3. The compound $[VO(acac)_2]$ 265 mg, 1.00 mmol) was added to a solution of *R*,*S*-H_3hidba (431 mg, 2.10 mmol) in MeOH (5 cm^3) and H_2O (10 cm^3). The reaction mixture was stirred (*ca.* 1 h) at 293 K, whereupon a blue-purple solution formed. The salt $[NH_4]_2[Ce(NO_3)_6]$ (630 mg, 1.15 mmol) was added, resulting in a dark red solution. A solution of $[PPh_4]Br$ (419 mg, 1.00 mmol) in CH_2Cl_2 (10 cm^3) was mixed with the aqueous phase and after rapid stirring (*ca.* 30 min) the dark red solution had transferred into the CH_2Cl_2 layer. This dark red solution was separated from the aqueous phase, then dried over anhydrous $CaCl_2$ (*ca.* 1 h) and evaporated to dryness under vacuum. The resulting residue was extracted into thf (10 cm^3) and filtered to remove any excess $[PPh_4]Br$. This solution was cooled (275 K) and added dropwise to cold (275 K) Et_2O (50 cm^3) to produce a pink precipitate. The solid product was very hygroscopic and therefore was collected in a dry dinitrogen atmosphere, washed with Et_2O (10 cm^3), dried under vacuum and stored under dinitrogen over silica gel. Yield 352 mg, 45% (Found: C, 60.49; H, 5.69; N, 3.45; P, 4.0. Calc. for $C_{40}H_{44}N_2O_{10}PV$: C, 60.45; H, 5.58; N, 3.52; P, 3.89%). IR (KBr, cm^{-1}): 1673 [ν(C=O)], 1384 [ν(C–O)] and 1149 cm^{-1} [ν(N–O)]. UV/VIS (CH_2Cl_2): ν/cm^{-1} (ε/dm^3 mol^{-1} cm^{-1}) 19 370 (243.5). NMR (CD_2Cl_2, 293 K): ^1H, δ 7.94–7.58 (m, 60 H, Ph), 4.98, 4.94, 4.78, 4.65, 4.36, 4.23 (6 m, 12 H, CH), 2.58–1.88 (m, 24 H, CH_2) and 1.15–1.03 (m, 36 H, CH_3); ^{13}C, δ 171.83, 170.89 (CO_2^-), 135.68–117.14 (Ph), 77.95, 76.96, 76.66, 75.97, 72.38, 71.21 (CH), 26.17, 26.10, 26.02, 24.03, 21.70, 20.77 (CH_2), 10.87, 10.37, 10.17 (CH_3); ^{51}V (313 K), δ −198, −235, −273. Mass spectrum (negative-ion FAB): *m*/*z* 455, [V(hidba)$_2$]$^-$.

X-Ray crystallography

A summary of the crystallographic data for compounds **1** and **2** is provided in Table 1. All data were corrected for Lorentz and polarisation effects and an empirical absorption correction, based on azimuthal scans of several reflections, was applied, using the program DIFABS.[21] The structures were solved by direct methods.[22] Hydrogen atoms were included in the structure factor calculations in idealised positions (C–H = 0.95 Å) and were assigned isotropic thermal parameters which were 20% greater than the equivalent *B* value of the atom to which they were bonded. All atoms which showed disorder were refined isotropically. The final cycle of full-matrix least squares, $\Sigma w(|F_o| - |F_c|)^2$, was based on the observed reflections [$I > 3.00\sigma(I)$] and the number of variable parameters, using neutral-atom scattering factors and anomalous dispersion corrections.[23]

Table 1 Crystal data for compounds **1** and **2**

	1	**2**
Formula	$C_{35}H_{66}Ca_2N_4O_{26}V_2$	$C_8H_{20}CaN_2O_{16}V$
M	1140.98	491.27
Crystal colour, habit	Blue, tabular	Blue, prismatic
Crystal dimensions/mm	0.30 × 0.20 × 0.10	0.05 × 0.15 × 0.25
Crystal system	Triclinic	Monoclinic
Space group	$P\bar{1}$ (no. 2)	$P2_1/c$ (no. 14)
a/Å	13.465(5)	8.509(3)
b/Å	20.519(6)	20.937(8)
c/Å	10.119(3)	10.376(3)
α/°	95.63(3)	
β/°	106.44(3)	109.77(2)
γ/°	73.18(3)	
U/Å^3	2566(1)	1739(1)
Z	2	4
D_c/g cm^{-3}	1.476	1.876
μ(Mo-Kα)/cm^{-1}	6.49	9.53
Diffractometer	Rigaku AFC5R	Rigaku AFC5R
Radiation λ/Å	0.71069 (graphite-monochromated)	0.71069 (graphite-monochromated)
T/K (±1)	296	294
Scan type	ω–2θ	ω
Scan rate/° min^{-1} (in ω)	8.0 (up to 3 scans)	8.0 (up to 3 scans)
Scan width/°	1.31 + 0.30 tan θ	0.84 + 0.30 tan θ
$2\theta_{max}$/°	51	55.1
No. of reflections measured: total, unique (R_{int})	9499, 9073 (0.035)	4756, 4146 (0.034)
No. of observations [$I > 3.00\sigma(I)$]	5300	3094
No. of variables	620	253
Residuals: R,R'	0.084, 0.083	0.038, 0.036
Goodness of fit indicator	3.30	1.83

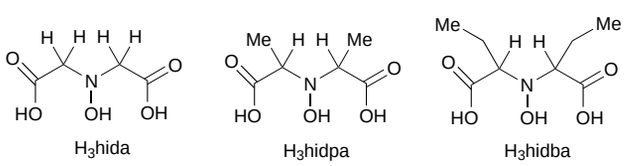

Fig. 1 A representation showing the pro-ligands H_3hida, H_3hidpa and H_3hidba

All calculations were performed using the TEXSAN[24] crystallographic software package.

CCDC reference number 186/738.

Results and Discussion

Ligand synthesis

The original preparations of the pro-ligands H_3hidpa [2,2′-(hydroxyimino)dipropionic acid] and H_3hida[17] involved solvent extraction steps, to isolate the compounds from the salt generated during the reactions, using absolute alcohol and glacial acetic acid, respectively. Crude products were precipitated from these solutions which contained sodium ions and gave hygroscopic, sticky residues at the end of the procedure. Further studies developed a more satisfactory technique for the separation of these pro-ligands from the reaction mixture, achieved *via* the precipitation of the zinc complexes.[18] These white precipitates were dissolved in dilute hydrochloric acid and absorbed onto strongly acidic cation exchange resin and the free (*N*-hydroxyimino)dicarboxylic acids were eluted with sodium hydroxide (*ca.* 0.2 mol dm^{-3}). The isolation of the new pro-ligand H_3hidba as a pure white crystalline compound has been achieved using a carefully selected solvent extraction and precipitation method (see Experimental section). This procedure exploits the increased alkyl bulk of H_3hidba, as compared to H_3hidpa and H_3hida, resulting in enhanced solubility in organic solvents and reduced solubility in H_2O. Fig. 1 shows a schematic representation of the three ligands H_3hida, H_3hidpa and H_3hidba. Proton and ^{13}C NMR spectra of H_3hidba show three

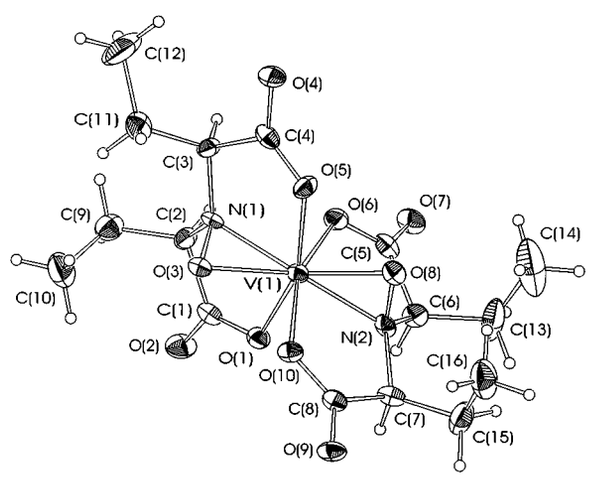

Fig. 2 Structure of the anion present in compound **1**

inequivalent proton and four inequivalent carbon resonances which can be attributed to the C_s symmetry of the molecule. Thus from a comparison of ^{1}H NMR spectra, the *R*,*S*-H_3hidba pro-ligand has been preferentially crystallised from a reaction mixture which contained the *R*,*R*-, *S*,*S*- and *R*,*S*-H_3hidba isomers in 1:1:2 ratio. The chemical implications of this new pro-ligand have been investigated and herein we report the characterisation of a new analogue of Amavadin.

New vanadium(IV) analogue of Amavadin

Compound **1**, involving a 1:2 complex of vanadium(IV) with *R*,*S*-H_3hidba, was isolated as blue tabular crystals in the space group $P\bar{1}$(no. 2) (Table 1). The complex anion in **1** contains the same overall structure as identified for $[NH_4][NMe_4][V(hida)_2]$[5] and Amavadin,[8] with vanadium(IV) co-ordinated to two mutually *trans* η^2-NO groups and four unidentate carboxylates (Fig. 2). The asymmetric unit consists of two $[V(hidba)_2]^{2-}$ anions linked *via* two Ca^{2+} cations to form a box-like arrangement (Fig. 3), where both vanadium centres are present as the Λ

Table 2 Comparison of selected vanadium–ligand bond lengths (Å) and angles (°) for compounds **1**, **2** and $[NH_4][NMe_4][V(hida)_2]$

			$[NH_4][NMe_4][V(hida)_2]$ (ref. 5)	
	1	**2**		
V(1)–O(1)	2.048(7)	2.061(2)	V(1)–O(1)	2.071(3)
V(1)–O(5)	2.040(7)	2.066(2)	V(1)–O(5)	2.065(3)
V(1)–O(6)	2.043(7)	2.078(2)	V(1)–O(6)	2.063(3)
V(1)–O(10)	2.044(6)	2.067(2)	V(1)–O(9)	2.070(3)
V(1)–O(3)	1.957(7)	1.940(2)	V(1)–O(3)	1.973(3)
V(1)–O(8)	1.935(7)	1.947(2)	V(1)–O(10)	1.976(3)
V(1)–N(1)	2.014(8)	2.018(3)	V(1)–N(1)	2.003(4)
V(1)–N(2)	2.007(8)	1.998(3)	V(1)–N(2)	2.002(3)
V(2)–O(11)	2.055(7)		O(3)–V(1)–N(1)	40.6(1)
V(2)–O(15)	2.062(7)		O(10)–V(1)–N(2)	40.6(1)
V(2)–O(16)	2.039(7)			
V(2)–O(20)	2.043(6)			
V(2)–O(13)	1.957(7)			
V(2)–O(18)	1.952(7)			
V(2)–N(3)	2.015(8)			
V(2)–N(4)	2.033(8)			
O(3)–V(1)–N(1)	40.0(2)	40.66(9)		
O(8)–V(1)–N(2)	40.5(3)	40.89(9)		
O(13)–V(2)–N(3)	40.6(3)			
O(18)–V(2)–N(4)	40.1(3)			

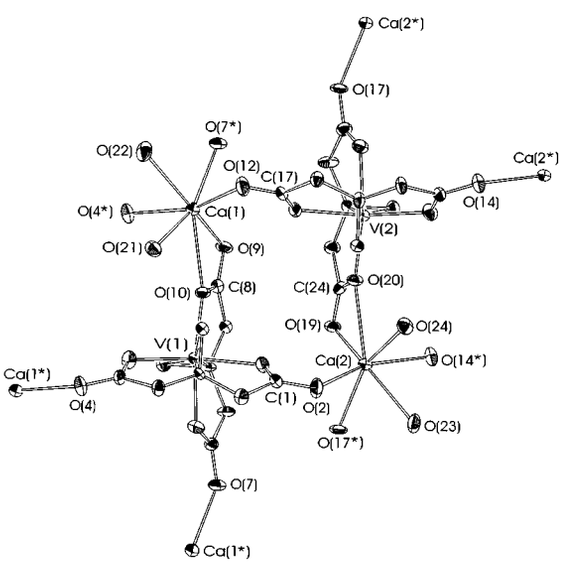

Fig. 3 Structure of the Ca_2V_2 centres in the asymmetric unit of compound **1**

helical form. The O(4*), O(7*), O(14*) and O(17*) oxygen atoms (Fig. 3) correspond to bonding from adjacent V_2Ca_2 units, similarly O(4) and O(7) bond to Ca(1*) atoms, with O(14) and O(17) co-ordinating to Ca(2*) atoms forming an extended structure of linked V_2Ca_2 boxes throughout the lattice (Fig. 4). This space group has a centre of symmetry, therefore the Δ handed complex is generated by symmetry and present in the unit cell. These connected V_2Ca_2 boxes form sheets in the crystal which stack in layers and each sheet contains strands of V_2Ca_2 units. These individual strands comprise V_2Ca_2 units which are exclusively the Δ or Λ hand at the vanadium centre and, as shown in Fig. 4, form along a horizontal axis through the crystal lattice. The view through the vertical plane of the lattice reveals a chain of linked vanadium and calcium centres, where the complex anions alternate between the Δ- and Λ-helical forms. Finally, there is a disordered H_2O and a molecule of isopropyl alcohol contained in the asymmetric unit which sit inbetween the layers of the crystal lattice. The purity of the bulk material was also confirmed by the 'clean' EPR spectra and cyclic voltammetric results (see below). The H_2O molecules

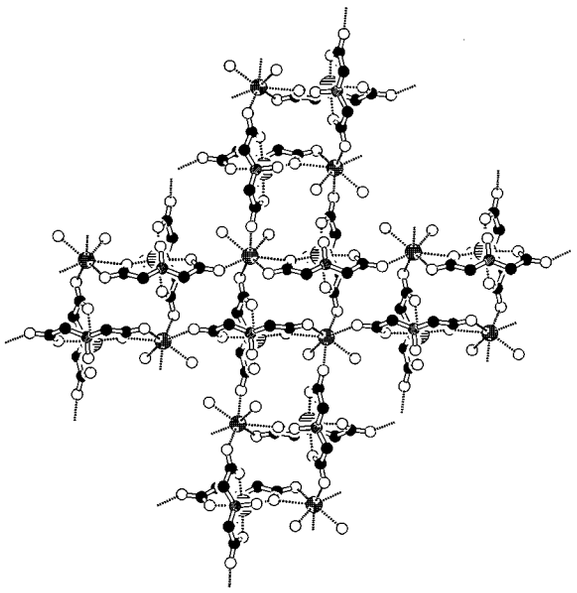

Fig. 4 Extended structural arrangement for compound **1**

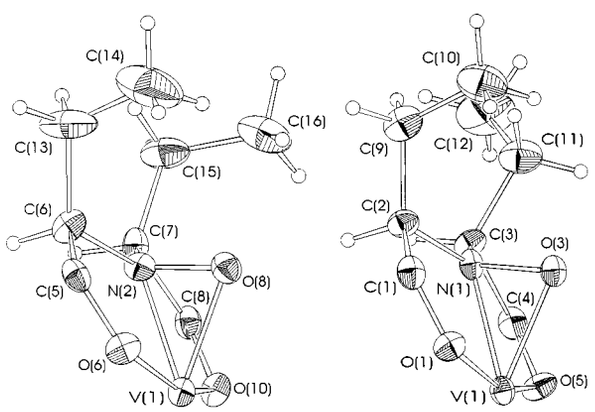

Fig. 5 View of the ethyl groups of the V(1) anion in compound **1**

occupy sites next to the Ca(1) centres, while the isopropyl alcohol molecules lie above and below the Ca(2) atoms. Also the *R*,*S* chirality of the ligand can be used as a lock on the structure solutions since this stereochemistry is carried directly through to the complex.

For complex **1** the V–O and V–N bond lengths and the angles subtended at the vanadium by the η^2-NO groups are comparable to those in its $[NH_4][NMe_4][V(hida)_2]$ counterpart (Table 2). The dihedral angles observed between the planes of the {VNO} groups (as illustrated in Scheme 1) are approximately perpendicular, 88.28 [V(1)] and 88.69° [V(2)], where the angles between the two N atoms are >90°. The planes of these {VNO} groups in each anion are almost perpendicular [V(1) 90.60 and 89.50°, V(2) 90.75 and 89.53°] to the least-squares plane of the vanadium and four oxygen-donor atoms of the unidentate carboxylate groups. These oxygen atoms are displaced from this least-squares plane; O(1) and O(5) sit below (−0.39 and −0.33 Å, respectively) and O(6) and O(10) sit above (0.39 and 0.32 Å, respectively) and O(11) and O(15) sit below (−0.40 and −0.32 Å, respectively) and O(16) and O(20) sit above (0.39 and 0.33 Å, respectively) the least-squares plane which contains the vanadium atom. Thus, the carboxylate-oxygen atoms from the same ligand are mutually *trans* and occupy sites on the same side of the least-squares plane thereby forming an alternation on the positions of these oxygen atoms with respect to the plane.

The ethyl groups of the ligands in the V(1) anion show two possible configurations (Fig. 5). The two ethyl groups attached to same ligand at the C(6) and C(7) atoms are approximately

Table 3 Comparison of Ca–O bond lengths (Å) for compounds **1** and **2**

1		**2**	
Ca(1)–O(21)	2.468(7)	Ca(1)–O(11)	2.467(3)
Ca(1)–O(22)	2.481(7)	Ca(1)–O(12)	2.379(2)
Ca(1)–O(12)	2.410(7)	Ca(1)–O(13)	2.465(2)
Ca(1)–O(4*)	2.378(7)	Ca(1)–O(14)	2.375(3)
Ca(1)–O(7*)	2.382(7)	Ca(1)–O(15)	2.412(2)
Ca(1)–O(9)	2.461(7)	Ca(1)–O(4)	2.410(2)
Ca(1)–O(10)	2.533(6)	Ca(1)–O(7*)	2.401(2)
Ca(2)–O(23)	2.493(7)		
Ca(2)–O(24)	2.434(7)		
Ca(2)–O(2)	2.410(7)		
Ca(2)–O(14*)	2.369(7)		
Ca(2)–O(17*)	2.381(7)		
Ca(2)–O(19)	2.441(7)		
Ca(2)–O(20)	2.544(6)		

Table 4 Comparison of adjacent O–Ca–O bond angles (°) for compounds **1** and **2**

1		**2**	
O(4*)–Ca(1)–O(7*)	91.4(2)	O(4)–Ca(1)–O(11)	79.68(8)
O(4*)–Ca(1)–O(9)	80.4(3)	O(4)–Ca(1)–O(12)	111.35(8)
O(4*)–Ca(1)–O(10)	87.6(2)	O(4)–Ca(1)–O(13)	77.14(8)
O(4*)–Ca(1)–O(21)	90.1(2)	O(4)–Ca(1)–O(14)	88.52(9)
O(4*)–Ca(1)–O(22)	78.6(3)	O(4)–Ca(1)–O(15)	88.98(8)
O(7*)–Ca(1)–O(9)	82.0(2)	O(7*)–Ca(1)–O(11)	101.57(8)
O(7*)–Ca(1)–O(12)	86.5(3)	O(7*)–Ca(1)–O(12)	75.67(8)
O(7*)–Ca(1)–O(22)	80.7(3)	O(7*)–Ca(1)–O(13)	105.83(8)
O(9)–Ca(1)–O(10)	51.9(2)	O(7*)–Ca(1)–O(14)	86.40(9)
O(9)–Ca(1)–O(12)	118.7(3)	O(7*)–Ca(1)–O(15)	84.86(8)
O(10)–Ca(1)–O(12)	108.1(2)	O(11)–Ca(1)–O(12)	85.99(9)
O(10)–Ca(1)–O(21)	72.4(2)	O(11)–Ca(1)–O(15)	72.23(8)
O(12)–Ca(1)–O(21)	83.5(2)	O(12)–Ca(1)–O(13)	69.65(8)
O(12)–Ca(1)–O(22)	81.7(3)	O(13)–Ca(1)–O(14)	72.21(9)
O(21)–Ca(1)–O(22)	74.4(3)	O(14)–Ca(1)–O(15)	72.43(8)
O(2)–Ca(2)–O(17*)	85.3(3)		
O(2)–Ca(2)–O(19)	118.8(3)		
O(2)–Ca(2)–O(20)	108.9(2)		
O(2)–Ca(2)–O(23)	81.2(2)		
O(2)–Ca(2)–O(24)	83.4(3)		
O(14*)–Ca(2)–O(17*)	95.5(3)		
O(14*)–Ca(2)–O(19)	81.4(2)		
O(14*)–Ca(2)–O(20)	85.4(2)		
O(14*)–Ca(2)–O(23)	78.9(2)		
O(14*)–Ca(2)–O(24)	87.1(2)		
O(17*)–Ca(2)–O(19)	81.9(2)		
O(17*)–Ca(2)–O(23)	79.9(2)		
O(19)–Ca(2)–O(20)	51.8(2)		
O(20)–Ca(2)–O(24)	73.2(2)		
O(23)–Ca(2)–O(24)	74.9(2)		

collinear, where the CH_2 groups [C(13) and C(15)] and the CH_3 groups [C(14) and C(16)] are eclipsed. However, the corresponding groups on the second *R*,*S*-hidba^{3-} moiety differ in the orientation at one of the CH_2 carbon atoms [C(9)] resulting in a staggered arrangement for the two CH_3 groups [C(12) and C(10)]. Two ethyl groups of different ligands in the V(2) molecule were disordered over two sites each.

The two Ca^{2+} centres in the asymmetric unit of **1** are each seven-co-ordinate (Fig. 3), containing two co-ordinated H_2O molecules [Ca(1)–O(21) and –O(22), Ca(2)–O(23) and –O(24)], three unidentate carboxylates [Ca(1)–O(12), –O(4*) and –O(7*), Ca(2)–O(2), –O(14*) and –O(17*)] and a bidentate carboxylate group [Ca(1)–O(9) and –O(10), Ca(2)–O(19) and –O(20)], see Table 3 for bond lengths. The O(10) and O(20) oxygen atoms in the bidentate carboxylates are simultaneously bound to the vanadium and calcium centres, where O(10) bridges V(1) and Ca(1) and O(20) bridges the V(2) and Ca(2) atoms. The angles subtended at the Ca atoms by adjacent Ca–O bonds range from 51.9(2) to 118.7(3)° for Ca(1) and 51.8(2) to 118.8(3)° for Ca(2) (Table 4). The most acute angles occur at the binding sites of bidentate carboxylate groups [O(9)–Ca(1)–O(10) and O(19)–Ca(2)–O(20)] and the largest angles are subtended by the adjacent carboxylate oxygen atoms from different anions [O(9)–Ca(1)–O(12) and O(2)–Ca(2)–O(19)].

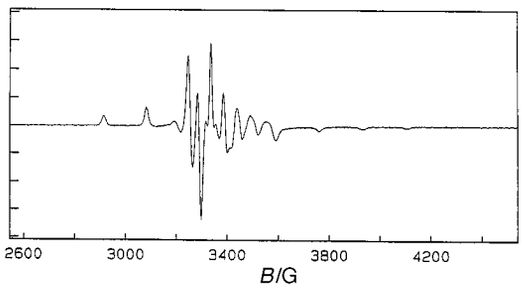

Fig. 6 X-Band frozen solution EPR spectrum of compound **1** (H_2O–glycerol, 120 K, $\nu = 9.45$ GHz)

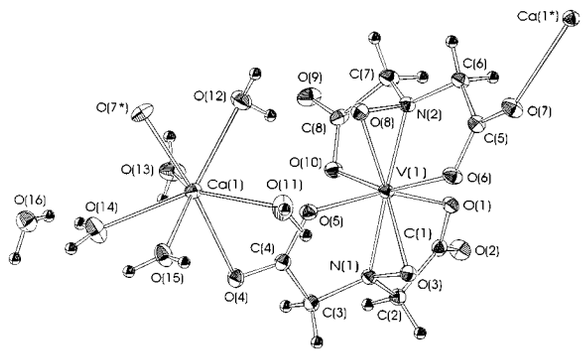

Fig. 7 Structure of the vanadium and calcium centres in the asymmetric unit of compound **2**

The electronic absorption spectrum obtained for **1** dissolved in H_2O showed two low intensity bands assigned to d–d transitions at $\nu = 17\,800$ and 12 900 cm^{-1}, the molar absorption coefficients are 25.3 and 14.8 $dm^3\ mol^{-1}\ cm^{-1}$, respectively, and an ill-defined band at $\nu = 13\,900\ cm^{-1}$ with a molar absorption coefficient of 15.2 $dm^3\ mol^{-1}\ cm^{-1}$. A very intense charge-transfer band in the region 35 000–39 000 cm^{-1} was also observed. The spectrum closely resembles the spectra obtained for Amavadin.[8] A comparison of the electronic structure of Amavadin with related compounds and VO^{2+} complexes, suggests a chemical[25] and an electronic[26] equivalence between the bonding of two mutually *trans* η^2-NO groups and one oxo group. By analogy with the electronic structure proposed for Amavadin and related systems from discrete variational (DV) Xα calculations,[26] the transitions observed for **1** at 12 900, 13 900 and 17 800 cm^{-1} are assigned as $d_{x^2-y^2} \longrightarrow d_{yx}$, d_{xz}, $d_{x^2-y^2} \longrightarrow d_{xy}$ and $d_{x^2-y^2} \longrightarrow d_{z^2}$, respectively.

The EPR spectrum of **1** was recorded in H_2O–glycerol at 120 K (Fig. 6). Direct comparison with the spectra obtained for Amavadin[8,27] indicated that the resonance positions are essentially the same. The X-band frozen solution spectrum appears rhombic and can be successfully simulated by the values $g_{zz} = 1.9220$, $g_{xx} = 1.9870$, $g_{yy} = 1.9830$ and $A_{zz} = 153 \times 10^{-4}$, $A_{xx} = 42 \times 10^{-4}$, $A_{yy} = 49 \times 10^{-4}\ cm^{-1}$ (*cf.* values obtained for Amavadin by Mabbs,[28] $g_{zz} = 1.9195$, $g_{xx} = 1.9848$, $g_{yy} = 1.9829$ and $A_{zz} = 154 \times 10^{-4}$, $A_{xx} = 43 \times 10^{-4}$, $A_{yy} = 48 \times 10^{-4}\ cm^{-1}$). This is consistent with the known structure of Amavadin with the highest possible point symmetry at the vanadium being C_2.

Compound **2** further highlights the novel interactions between these Amavadin-style complexes and Ca^{2+} cations giving rise to some distinctive crystallographic features. Other examples include analogous titanium and zirconium compounds.[16] Compound **2** crystallises as blue prisms in the space group $P2_1/c$ (no. 14) (Table 1). As expected the complex anion exhibits the Amavadin-style eight-co-ordinate geometry, see Fig. 7. This structure consists of alternate linked $[Ca(H_2O)_5]^{2+}$

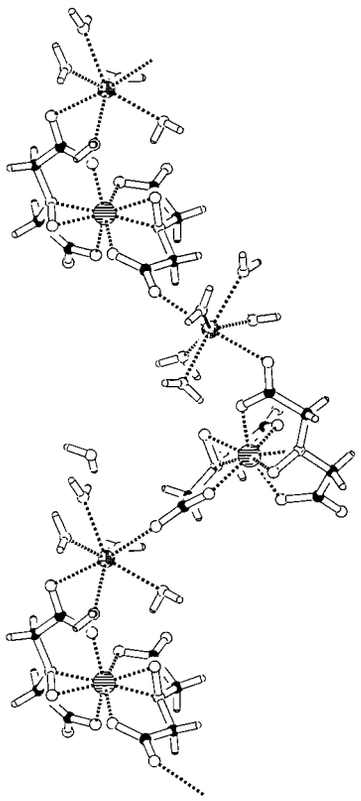

Fig. 8 Extended structural arrangement for compound **2**

and $[V(hida)_2]^{2-}$ units forming infinite helical chains, in the asymmetric unit $[V(hida)_2]^{2-}$ bonds to two Ca^{2+} centres [Ca(1) and Ca(1*)] *via* a carboxylate group on each $hida^{3-}$ ligand at the O(4) and O(7) atoms (Fig. 7). Both isomers at the vanadium centre are present in the unit cell, where the $[V(hida)_2]^{2-}$ units are alternately the Δ and Λ hands through the helical chain (Fig. 8). Refinement was carried out for the Λ form in the asymmetric unit as shown in Fig. 7. The vanadium–ligand bond lengths are comparable to both those in **1** and the previously reported $[NH_4][NMe_4][V(hida)_2]$ (Table 2). The η^2-NO groups subtend angles at the vanadium which are similar to these counterparts (Table 2) and the planes of these two groups are close to mutually perpendicular (90.72°). Each {VNO} plane is effectively perpendicular (91.22 and 87.98°) to the least-squares of the vanadium and the four carboxylate oxygen donor atoms. As in **1** these oxygen atoms show similar displacement from this least-squares plane; O(1) and O(5) sit below (−0.43 and −0.34 Å, respectively) and O(6) and O(10) sit above (0.35 and 0.49 Å, respectively) the plane containing the vanadium.

As in **1** each Ca^{2+} cation is seven-co-ordinate, however, in **2** the co-ordination sphere of the calcium is slightly different, comprised of five bonded H_2O molecules [O(11), O(12), O(13), O(14) and O(15)] and two unidentate carboxylate groups bound through the O(4) and O(7*) oxygen atoms {O(7*) is from the adjacent $[V(hida)_2]^{2-}$ anion in the helical chain}, see Table 3 for bond lengths. The angles subtended at the Ca atom by adjacent Ca–O bonds range from 69.65(8)° [O(12)–Ca(1)–O(13)] to 111.35(8)° [O(4)–Ca(1)–O(12)] (Table 4). In contrast to **1** no bridging between the calcium and vanadium centres is observed *via* bidentate carboxylate groups. Finally, an extra sixth H_2O molecule [O(16)], not co-ordinated to Ca(1), is present in the crystal lattice hydrogen bonded to the O(14) H_2O molecule (Fig. 7).

Cyclic voltammetric studies and the vanadium(V) analogue

Table 5 lists the $E_{\frac{1}{2}}$ values of the V^V–V^{IV} process reported in literature for the cyclic voltammograms of Amavadin and $[V(hida)_2]^{2-}$ using H_2O or Me_2SO as solvents, where a reduction

Table 5 The $E_{\frac{1}{2}}$ values recorded in different solvents at a platinum bead working electrode (*vs.* SCE) for compounds **1**, **3** and related vanadium analogues

		V^V–V^{IV}		
Compound	Solvent–electrolyte	$E_{\frac{1}{2}}$/V	Δ*E*/mV	$i_{pa}:i_{pc}$
1	H_2O–KCl	+0.43	70	0.94
	Me_2SO-$[NBu^n_4][BF_4]$	−0.07	80	0.98
3	CH_2Cl_2-$[NBu^n_4][BF_4]$	−0.09	80	1.02
$H_2[V(hida)_2]$ (ref. 6)	H_2O-KCl	+0.65		
	Me_2SO-$[NBu^n_4][BF_4]$	+0.14		
Amavadin (ref. 6)	H_2O-KCl	+0.53		
	Me_2SO-$[NBu^n_4][BF_4]$	+0.03		

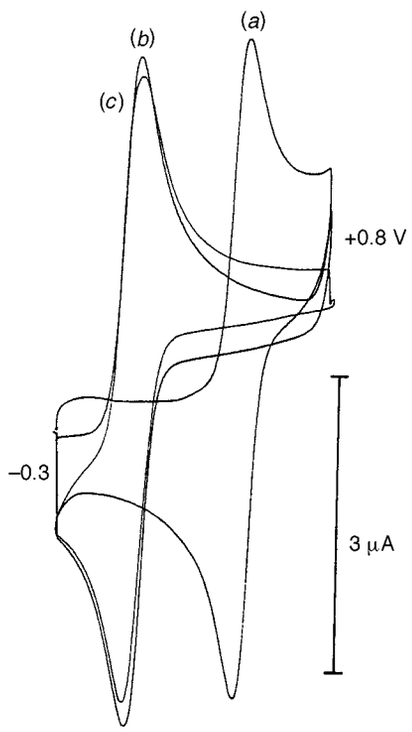

Fig. 9 Cyclic voltammograms recorded at a platinum bead electrode (*vs.* SCE) for compounds **1** (*a*), (*b*) and **3** (*c*) (*ca.* 1 mmol dm^{-3}) with a variety of solvent-supporting electrolyte systems {(*a*) = H_2O–KCl, (*b*) = Me_2SO–$[NBu^n_4][BF_4]$, (*c*) = CH_2Cl_2–$[NBu^n_4][BF_4]$, *ca.* 0.2 mol dm^{-3}}. The voltammograms shown were recorded at 293 K with a scan rate of 200 mV s^{-1}, in each case the current peak intensity (i_p) obeys a linear relationship with the square root of the scan rate (range: 20–700 mV s^{-1})

of *ca.* 500 mV is observed when switching from aqueous to organic solutions.[6] Recent crystallographic studies[8] with Amavadin crystallised from H_2O, have shown how the complex anion interacts with the solvent molecules through hydrogen bonding, *via* the non-ligating carboxylate-oxygen atom of the ligand. This influence is detected in the cyclic voltammetric experiment, resulting in higher redox potentials in H_2O compared with Me_2SO for the V^V–V^{IV} couple. The nature of the ligand also affects the observed potential of the V^V–V^{IV} couple and an increase of >100 mV in the recorded $E_{\frac{1}{2}}$ value is detected between the voltammograms of Amavadin and $[V(hida)_2]^{2-}$,[6] in both solvents (Table 5). This corresponds with the expected stronger electron-donating ability of $hidpa^{3-}$ relative to $hida^{3-}$.

The non-innocent roles played by the ligand–solvent interactions in the redox potentials of these complexes have been explored further with **1**. Fig. 9(*a*) and 9(*b*) show the cyclic voltammograms recorded for **1** in H_2O and Me_2SO under identical conditions to the previous experiments with the analogous

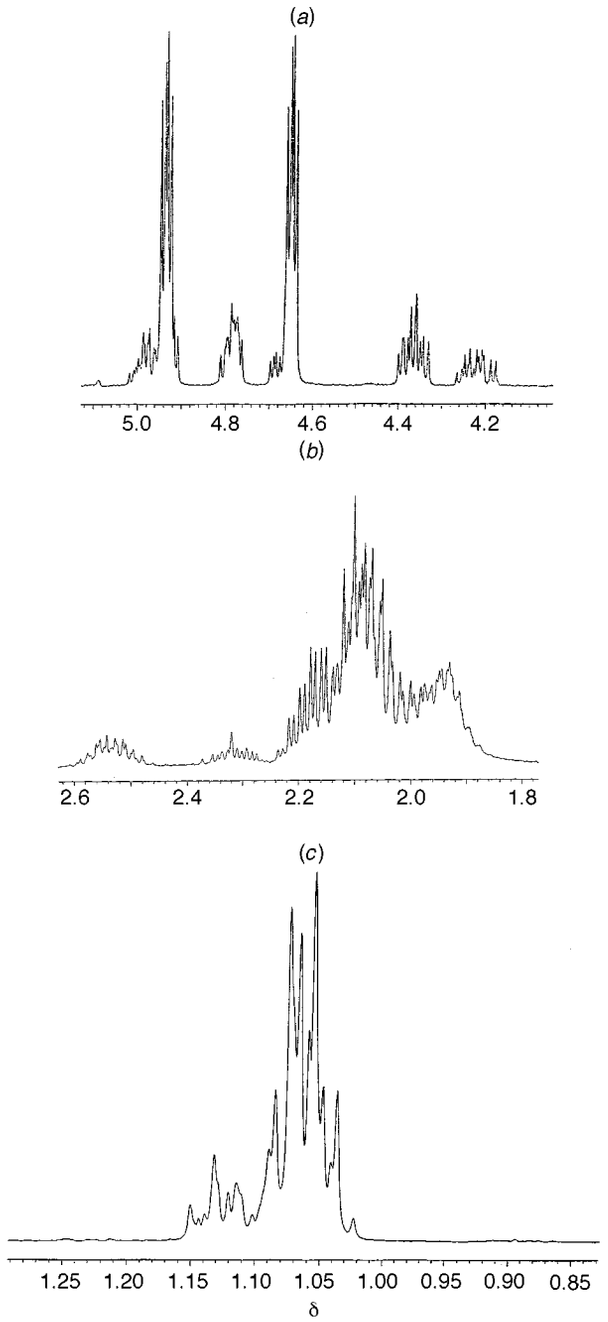

Fig. 10 Proton NMR (300 MHz, CD_2Cl_2, 293 K) spectrum recorded for compound **3**, (*a*) = CH region, (*b*) = CH_2 region, (*c*) = CH_3 region

complexes and the $E_{\frac{1}{2}}$ values are listed in Table 5. In both solvents the V^V–V^{IV} redox couples recorded for **1** behaved as reversible one-electron processes. The redox properties of **1** are consistent with that of Amavadin and $[V(hida)_2]^{2-}$, with a reduction of 500 mV between the $E_{\frac{1}{2}}$ values recorded in Me_2SO relative to H_2O. As expected the observed potential of the V^V–V^{IV} couple correlates with the stronger electron-releasing ability of $hidba^{3-}$ relative to $hidpa^{3-}$ and $hida^{3-}$. The $E_{\frac{1}{2}}$ values recorded in H_2O and Me_2SO show a reduction of 100 mV for **1** compared to Amavadin, and a decrease of 220 and 210 mV, respectively, for **1** relative to $[V(hida)_2]^{2-}$ (Table 5). The increased electron-donating ability of H_3hidba has enhanced the stability of the higher oxidation state of **1** and in Me_2SO the V^V state is thermodynamically preferred. It should also be noted that da Silva *et al.*[29] have proposed a Michaelis–Menten type mechanism for the electrocatalytic oxidation of mercaptocarboxylic acids by an Amavadin model.

The chemical oxidation of **1** in H_2O was achieved using ammonium ceric nitrate to yield a dark red solution, which was

Table 6 Comparison of ^{13}C NMR (300 MHz, CD_2Cl_2, 293 K) resonances for compound **3** with related vanadium and niobium complexes

	δ			
Compound	CO_2^-	CH	CH_2	CH_3
3	171.83	77.95	26.17	10.87
	170.89	76.96	26.10	10.37
		76.66	26.02	10.17
		75.97	24.03	
		72.38	21.70	
		71.21	20.77	
$[V(R,S\text{-hidpa})_2]^-$	174.23	72.56		19.35
(ref. 8)	174.15	72.44		16.23
	173.28	72.27		16.11
	173.06	71.68		16.06
	172.97	71.52		15.01
	172.09	71.29		14.19
$[Nb(R,S\text{-hidpa})_2]^-$	175.66	68.63		19.04
(ref. 15)	174.52	68.57		18.94
	174.43	68.42		18.91
	174.37	68.29		15.91
	174.29	68.20		15.71
	173.96	68.11		13.99

transferred into CH_2Cl_2 with $[PPh_4]Br$ and **3** was precipitated upon addition to cold (275 K) Et_2O. Proton, ^{13}C and ^{51}V NMR spectroscopy have been used to study **3** in CD_2Cl_2. The assignment of these NMR data is consistent with C_2 point symmetry of the eight-co-ordinate anion in solution and by analogy with the $[V(R,S\text{-hidpa})_2]^-$[8] and $[Nb(R,S\text{-hidpa})_2]^-$[15] complexes, **3** has three possible enantiomeric pairs. If all the potential diastereomers are present in solution then six inequivalent ^1H and ^{13}C environments are anticipated in each region of the spectrum.[8] Fig. 10 shows the ^1H NMR spectrum obtained for **3** and the small chemical shift differences between the various resonances due to the individual diastereomers present caused extensive overlap of the peaks. Each diastereomer is expected to give rise to two triplets for the CH groups, two doublets of quartets due to CH_2 and two triplets from the CH_3 resonances. This overlap inhibits detailed assignment of the spectrum, where the CH_2 (δ 2.58–1.88) [Fig. 10(*b*)] and CH_3 (δ 1.15–1.03) [Fig. 10(*c*)] regions appear as multiplets. However, the CH resonances produced a series of well resolved multiplets between δ 4.98 and 4.23 [Fig. 10(*a*)]. These data suggest that one diastereomer dominates in solution since the integrals of the two multiplets centred at δ 4.94 and 4.65 are substantially larger than the other multiplets. Table 6 lists the ^{13}C resonances observed for **3** and its vanadium and niobium counterparts. As observed in the ^1H NMR spectrum, these data are consistent with the overall presence of three diastereomers of **3**, where the CH, CH_2 and CH_3 carbon environments each showed a collection of peaks. However, the lower intensity of the CO_2^- carbon resonances means that only the two resonances due to the dominant diastereomer were observed. The high thermal motion of the CH_3 groups, observed in the crystal structure of **1**, results in coincidence of these carbons, producing two intense resonances (δ 10.17 and 10.37) and a smaller peak (δ 10.87) in this region of the spectrum. The ^1H–^{13}C correlation spectrum of **3** showed that the carbon resonances of greatest intensity at δ 76.66, 75.97, 26.17, 26.02, 10.37 and 10.17 correlate to the proton signals at δ 4.94, 4.65, 2.11, 2.07, 1.08 and 1.05, respectively. The ^{51}V NMR spectrum recorded for **3** at 313 K confirmed the presence of three diastereomers in solution and further established retention of molecular geometry in solution, showing three inequivalent resonances at δ −198, −235 and −273 *vs.* $VOCl_3$. The $[PPh_4]$-$[\Delta\text{-}V(S,S\text{-hidpa})_2]$ and $[PPh_4][V(hida)_2]$ compounds showed single ^{51}V resonances at δ −281 and −263, respectively.[9] As

with **3**, $[PPh_4][\Delta,\Lambda\text{-}V(R,S\text{-hidpa})_2]$ displayed three analogous ^{51}V resonances at δ −250, −270 and −280.[8]

Fig. 9(*c*) shows the cyclic voltammogram recorded for **3** in CH_2Cl_2, which displays a similar reversible V^V–V^{IV} redox couple to **1** (Table 5). The electronic absorption spectrum obtained for **3** in CH_2Cl_2 showed no low intensity d–d transitions which is consistent for the d^0 configuration of the vanadium(v) state. However, the spectrum is dominated by a medium intensity charge-transfer band from the ligand into the empty d orbitals, observed at $\nu = 19\,370$ cm^{-1} with a molar absorption coefficient of 243.5 dm^3 mol^{-1} cm^{-1}. This can be assigned by comparison with previous studies with oxidised Amavadin ($\nu = 19\,900$ cm^{-1}, $\varepsilon = 216.6$ dm^3 mol^{-1} cm^{-1}),[8] where the computed transition energies showed that this band may arise from carboxylate ⟶ vanadium and/or O_{NO} ⟶ vanadium transitions.[26] A further very intense band was shown in the 35 000–39 000 cm^{-1} region. The infrared spectrum of **3** displays a shift in the [ν(C=O)] stretching frequency relative to **1**, where an increase of 60 cm^{-1} is observed on oxidation to the vanadium(v) state. A similar shift in the [ν(C=O)] stretching frequency was observed from 1625 to 1672 cm^{-1} upon oxidation of Amavadin,[8] which is consistent with a modest contraction of the bond lengths.

Conclusion

The syntheses of H_3hidba and **1** have highlighted that further analogues of Amavadin are possible and increasing the alkyl bulk on the periphery of the pro-ligand has an influence on the chemical and structural properties of these compounds. As this R group is increased in length the interaction with organic solvents (solubility) will be enhanced, also the increased electron-releasing ability of $hidba^{3-}$ leads to a stabilisation of the vanadium(v) state in non-co-ordinating organic media. Single crystal X-ray diffraction studies showed the same eight-co-ordinate geometry for the molecular anions of **1** and **2** as identified for Amavadin and related complexes. However, the interaction of these anions with Ca^{2+} atoms revealed some intriguing crystallographic features producing two very distinct extended solid-state structures in the crystal lattice. Chemical oxidation of **1** to yield **3** provided a probe into the NMR properties of this new complex.

Acknowledgements

We thank British Nuclear Fuels plc (BNFL) for funding (to P. D. S. and S. M. H.), EPSRC for funding (to R. E. B.), Dr. E. J. L. McInnes (EPSRC CW EPR Service Centre, Department of Chemistry, The University of Manchester) for EPR spectra, Mr. J. Friend for assistance with NMR studies (Department of Chemistry, The University of Manchester) and Dr. P. Harston (Company Research Laboratories, BNFL, Springfields, Preston, Lancashire) for valuable discussions during the course of this work. D. C. thanks The Royal Society for financial support.

References

1 H. U. Meisch, W. Reinle and J. A. Schmitt, *Naturwissenchaften*, 1979, **66**, 620.
2 E. Bayer and H. Kneifel, *Z. Naturforsch.*, *Teil B*, 1972, **27**, 207.
3 H. Kneifel and E. Bayer, *Angew. Chem.*, *Int. Ed. Engl.*, 1973, **12**, 508.
4 H. Kneifel and E. Bayer, *J. Am. Chem. Soc.*, 1986, **108**, 3075.
5 M. A. A. F. de C. T. Carrondo, M. T. L. S. Duarte, J. C. Pessoa, J. A. L. Silva, J. J. R. Fraústo da Silva, M. C. T. A. Vaz and F. L. Vilas-Boas, *J. Chem. Soc.*, *Chem. Commun.*, 1988, 1158.
6 M. A. Nawi and T. L. Riechel, *Inorg. Chim. Acta*, 1987, **136**, 33.
7 J. J. R. Fraústo da Silva, M. F. C. G. da Silva, J. A. L. da Silva and A. J. L. Pombeiro, *in Molecular Electrochemistry of Inorganic, Bioinorganic and Organometallic Compounds*, eds. A. J. L. Pombeiro and J. A. McCleverty, Kluwer, Dordrecht, 1993, p. 411.
8 E. M. Armstrong, M. S. Austerberry, D. Collison, S. N. Ertok, C. D. Garner, M. Helliwell and F. E. Mabbs, unpublished work; S. N. Ertok, Ph.D. Thesis, The University of Manchester, 1993.
9 E. M. Armstrong, R. L. Beddoes, L. J. Calviou, J. M. Charnock, D. Collison, S. N. Ertok, J. H. Naismith and C. D. Garner, *J. Am. Chem. Soc.*, 1993, **115**, 807.
10 E. M. Armstrong, L. J. Calviou, J. M. Charnock, D. Collison, S. N. Ertok, C. D. Garner, F. E. Mabbs and J. H. Naismith, *J. Inorg. Biochem.*, 1991, **43**, 413; L. J. Calviou, Ph.D. Thesis, The University of Manchester, 1992.
11 J. J. R. Fraústo da Silva, *Chem. Speciation Bioavailability*, 1989, **1**, 139.
12 R. D. Thackrey and T. L. Riechel, *J. Electroanal. Chem. Interfacial Electrochem.*, 1988, **245**, 131.
13 H. S. Yadav, E. M. Armstrong, R. L. Beddoes, D. Collison and C. D. Garner, *J. Chem. Soc.*, *Chem. Commun.*, 1994, 605.
14 P. D. Smith, E. J. L. McInnes, R. L. Beddoes, D. Collison, J. J. A. Cooney, S. M. Harben, M. Helliwell, F. E. Mabbs, A. K. Powell and C. D. Garner, unpublished work.
15 P. D. Smith, S. M. Harben, R. L. Beddoes, M. Helliwell, D. Collison and C. D. Garner, *J. Chem. Soc.*, *Dalton Trans.*, 1997, 685.
16 S. M. Harben, P. D. Smith, R. L. Beddoes, D. Collison and C. D. Garner, *Angew. Chem.*, *Int. Ed. Engl.*, 1997, **36**, 1897.
17 J. Felchman, M. Cândida, T. A. Vaz and J. J. R. Fraústo da Silva, *Inorg. Chim. Acta*, 1984, **93**, 101.
18 E. Koch, H. Kneifel and E. Bayer, *Z. Naturforsch.*, *Teil B*, 1986, **41**, 359; G. Anderegg, E. Koch and E. Bayer, *Inorg. Chim. Acta*, 1987, **127**, 183.
19 C. J. Pickett, *J. Chem. Soc.*, *Chem. Commun.*, 1985, 323.
20 R. R. Gagné, G. A. Konal and G. C. Lisensky, *Inorg. Chem.*, 1980, **19**, 2854.
21 N. Walker and D. Stewart, *Acta. Crystallogr.*, *Sect. A*, 1983, **39**, 158.
22 G. M. Sheldrick, SHELXS 86, *Crystallographic Computing 3*, eds. G. M. Sheldrick, C. Krueger and R. Goddard, Oxford University Press, 1986.
23 D. T. Cromer and J. T. Waber, *International Tables for X-Ray Crystallography*, The Kynoch Press, Birmingham, 1974, vol. 4, Table 2.2A and 2.3.1.
24 TEXSAN-TEXRAY, Structure Analysis Package, Molecular Structure Corporation, Houston, TX, 1985.
25 D. Collison, *J. Inorg. Biochem.*, 1991, **43**, 403.
26 E. M. Armstrong, D. Collison, R. J. Deeth and C. D. Garner, *J. Chem. Soc.*, *Dalton Trans.*, 1995, 191.
27 R. D. Gillard and R. J. Lancashire, *Phytochemistry*, 1984, **23**, 179; E. Koch, H. Kneifel and E. Bayer, *Z. Naturforsch.*, *Teil C*, 1987, **42**, 873; P. Krauss, E. Bayer and H. Kneifel, *Z. Naturforsch.*, *Teil B*, 1984, **39**, 829; G. Bemski, J. Felcman, J. J. R. Fraústo da Silva, I. Moura, M. C. T. A. Vaz and L. F. Vilas-Boas, *Rev. Port. Quim.*, 1985, **27**, 418; G. Bemski, J. Felcman, J. J. R. Fraústo da Silva, I. Moura, M. C. T. A. Vaz and L. F. Vilas-Boas, *Frontiers in Bioinorganic Chemistry*, ed. A. V. Xavier, VCH, Weinheim, New York, Basel, Cambridge, Tokyo, 1986, pp. 97–105.
28 F. E. Mabbs, *Chem. Soc. Rev.*, 1993, **22**, 313.
29 M. F. C. G. da Silva, J. A. L. da Silva, J. J. R. Fraústo da Silva, A. J. L. Pombeiro, C. Amatore and J.-N. Verpeaux, *J. Am. Chem. Soc.*, 1996, **118**, 7568.

Received 28*th May* 1997; *Paper* 7/03683C